CANCER RESEARCH COMMUNICATIONS

AACR American Association for Cancer Research

RESEARCH ARTICLE https://doi.org/10.1158/2767-9764.CRC-23-0013 OPEN ACCESS

Deconstructing Olfactory Epithelium Developmental Pathways in Olfactory Neuroblastoma

John B. Finlay[1,2,3], Ralph Abi Hachem[2], David W. Jang[2], Nosayaba Osazuwa-Peters[2], and Bradley J. Goldstein[2,3,4]

ABSTRACT

Olfactory neuroblastoma is a rare tumor arising from the olfactory cleft region of the nasal cavity. Because of the low incidence of this tumor, as well as an absence of established cell lines and murine models, understanding the mechanisms driving olfactory neuroblastoma pathobiology has been challenging. Here, we sought to apply advances from research on the human olfactory epithelial neurogenic niche, along with new biocomputational approaches, to better understand the cellular and molecular factors in low- and high-grade olfactory neuroblastoma and how specific transcriptomic markers may predict prognosis. We analyzed a total of 19 olfactory neuroblastoma samples with available bulk RNA-sequencing and survival data, along with 10 samples from normal olfactory epithelium. A bulk RNA-sequencing deconvolution model identified a significant increase in globose basal cell (GBC) and CD8 T-cell identities in high-grade tumors (GBC from ∼0% to 8%, CD8 T cell from 0.7% to 2.2%), and significant decreases in mature neuronal, Bowman's gland, and olfactory ensheathing programs, in high-grade tumors (mature neuronal from 3.7% to ∼0%, Bowman's gland from 18.6% to 10.5%, olfactory ensheathing from 3.4% to 1.1%). Trajectory analysis identified potential regulatory pathways in proliferative olfactory neuroblastoma cells, including PRC2, which was validated by immunofluorescence staining. Survival analysis guided by gene expression in bulk RNA-sequencing data identified favorable prognostic markers such as SOX9, S100B, and PLP1 expression.

Significance: Our analyses provide a basis for additional research on olfactory neuroblastoma management, as well as identification of potential new prognostic markers.

Introduction

Olfactory neuroblastoma (ONB), also referred to as esthesioneuroblastoma, is a rare neoplasm that is thought to arise from the olfactory epithelium (OE) in the superior nasal cavity. ONB, first described in 1924, accounts for approximately 2%–3% of sinonasal malignancies (1, 2). Given the location of the tissue of origin, local growth of ONBs can invade superiorly into the anterior skull base and brain, laterally into the orbit, or inferiorly into the inferior nasal cavity and paranasal sinuses. ONB can also metastasize to the cervical lymph nodes and distant sites. Historically, ONBs have been graded pathologically using the Hyams system, which takes into account Ki-67 proliferative index and presence of necrosis (3, 4). Stage is typically determined using either the Kadish or Dulguerov system, both of which assess the extent of local primary tumor extension to the paranasal sinuses or cranial cavity, and the presence of local metastasis (5, 6). Patients can present with epistaxis, nasal congestion, olfactory loss, visual changes, headache, and in advanced disease, weight loss.

The standard of care for ONB, which has remained relatively unchanged for decades, is surgical resection followed by radiotherapy (7, 8). Chemotherapy has often been added for advanced disease (9). Even with aggressive surgical and medical management, the 2-year survival rate of high grade ONBs remains steady at approximately 40%, and late recurrences can occur (10).

Because of their extremely low incidence of 0.4 in 1 million, large detailed studies of ONB have been a challenge, although case series and systematic reviews have provided insights (11, 12). No reliable mouse models or patient-derived cell lines exist, making it difficult to experimentally manipulate tumor biology. In addition, the precise mechanisms driving proliferation and differentiation in the adult OE, which actively produces new neurons throughout life from resident basal stem cells, remain an area of active research. Thus, it has been difficult to contextualize the neoplastic processes driving ONB growth with regard to the specific cell identities of the OE. Because of these limitations, the use of targeted and/or immune-modulating therapies has not been established in the treatment for ONB, in contrast to other cancers.

[1]Medical Scientist Training Program, Duke University School of Medicine, Durham, North Carolina. [2]Department of Head and Neck Surgery & Communication Sciences, Duke University, School of Medicine, Durham, North Carolina. [3]Department of Cell and Molecular Biology, Duke University School of Medicine, Durham, North Carolina. [4]Department of Neurobiology, Duke University School of Medicine, Durham, North Carolina.

Corresponding Author: Bradley J. Goldstein, Duke University School of Medicine, DUMC 3805, Durham, NC 27710. Phone: 919-684-6595; E-mail: bradley.goldstein@duke.edu

doi: 10.1158/2767-9764.CRC-23-0013

Recent advances in human olfactory stem cell biology offer a new lens through which to study ONB (13). The adult OE is a dynamic neurogenic niche that allows for constant production of sensory neurons, sustentacular support cells, microvillar cells, and glands throughout life (14–17). The embryonic origin of the OE is largely derived from a cranial sensory ectodermal placode, while the underlying lamina propria, housing glands, vessels, and olfactory ensheathing glia cells, arises from cranial neural crest (18). However, mouse genetic lineage tracing studies identified evidence for intermixing of placode and neural crest, reflecting the complexities of the origins of the peripheral olfactory structures in mammals (18). In adults, a reserve population of quiescent stem cells, termed horizontal basal cells (HBC), lines the basal lamina of the OE, and can become activated by epithelial damage to generate proliferative globose basal cells (GBC). GBCs are heterogenous and function as amplifying neuronal progenitors or immediate neuronal precursor (INP) cells that differentiate rapidly into immature olfactory sensory neurons (iOSN) or microvillar cells; there is also a direct lineage relationship between GBCs and submucosal Bowman's glands.

It has been suggested that high-grade ONBs arise from proliferative basal cells, with less aggressive tumors having more neuronal characteristics (19). However, this does not take into account the diversity of differentiation trajectories and proliferative cell states within the normal OE. The expression of glandular proteins within ONB has also been reported, suggesting that tumors may be more heterogenous than originally thought (20). An olfactory neuronal lineage origin for ONB has been supported strongly by identification of neuronal antigens such as neurofilament in the tumors (21), or by identification of GBC-specific transcription factors such as ASCL1 (22). More recent molecular analyses have also suggested the expression of neural crest transcripts using bulk RNA sequencing (RNA-seq; ref. 19), although this approach cannot provide cell type–specific resolution. As such, the cellular and molecular mechanisms driving ONB growth remain incompletely understood.

Here, we take advantage of an integrated single-cell transcriptomic atlas of the human olfactory mucosa, which we previously generated using human biopsy samples, to deconvolute bulk RNA-seq expression patterns in 19 publicly available ONB samples and three control samples. Our findings indicate that GBCs are significantly enriched in higher grade tumors, as expected. Differentiation trajectory analysis in normal OE cells reveals that components of the polycomb repressive complex 2 (PRC2), a conserved epigenetic regulatory structure, are enriched in both GBC and iOSN states. We perform here immunostaining confirming that PRC2 proteins are associated with proliferative cells in ONB, even in low-grade tumors. We find that lower grade tumors are enriched for olfactory ensheathing cell and Bowman's gland transcripts, and that expression of canonical markers for these cell identities is positively correlated with overall survival. Guided by perspectives from adult olfactory cell biology, this analysis provides novel insights into factors active in ONB tumors, suggesting important mechanisms contributing to tumor growth and outcome, as well as pathologic markers for prognosis.

Materials and Methods

Bioinformatics

Preprocessing of Bulk RNA-seq Samples

Bulk RNA-seq datasets were queried from the NCBI Gene Expression Omnibus (GEO) from GSE118995 (19 ONB samples; ref. 19), and GSE80249 (three normal OE samples; ref. 23). FASTQ files for each patient sample were downloaded and imported into Galaxy (v22.05.1) via the Sequence Read Archive (SRA) for processing. Low-quality sequencing reads were trimmed from paired-end data using Trimmomatic (v0.38.0) with default settings and no Illumina barcode trimming. Trimmed datasets were then aligned to hg19 using HISAT2 (v2.2.1) with default settings. Counts per gene were calculated with featureCounts (v2.0.1) with "Count fragments instead of reads" enabled under "options for paired-end reads," and all other default settings. Finally, annotateMyIDs (v3.14.0) was used to link Entrez IDs to Gene names.

Bulk RNA-seq Deconvolution

Deconvolution of bulk RNA-seq datasets with an integrated single-cell RNA-seq (scRNA-seq) reference dataset was performed in Python (v3.9.0) using Scanpy (v1.9.1). scRNA-seq datasets used as a reference in the deconvolution model were imported from GSE139522 (13) and GSE184117 (24). Specifically, we used all 4 patients from Durante and colleagues, 2020 (31,631 cells) and the 3 normosmic patients from Oliva and colleagues, 2021 (19,620 cells). Datasets were processed, integrated using scvi-tools (v0.17.4), and annotated by cell type cluster, as described previously (25).

For deconvolution, we utilized RNA-Sieve (v0.1.4; ref. 26). Once an integrated scRNA-seq dataset was properly annotated by cell type, we subset this to include only the four olfactory mucosal biopsies from Durante and colleagues, 2020 due to computing constraints of using all seven datasets simultaneously as a reference. When the model was run with the three normal olfactory mucosal biopsies from Oliva and colleagues, 2021 as reference, similar predicted output proportions were observed. A concatenated counts matrix with counts from all 19 ONB and three normal OE bulk RNA-seq dataset was imported. We eliminated genes only present in either the scRNA-seq dataset or the bulk RNA-seq datasets using index.intersection(). Raw counts for scRNA-seq and bulk RNA-seq datasets were prepped for running the deconvolution model with default settings, as described previously (26). The deconvolution model was trained by running model_from_raw_counts() on the processed scRNA-seq reference dataset. Then the model was run with model.predict(), using default settings. Output graphs were produced using Altair (v4.2.0). Statistical comparisons between predicted cell-type proportions were run in Graphpad Prism 9.

Trajectory Analysis and Plots

Trajectory analysis was performed using Scanpy (v1.9.1) and the integrated scRNA-seq dataset with seven normal human olfactory mucosa biopsies, described above. First, we subset out just olfactory epithelial clusters (HBCs, GBCs, INPs, iOSN, mOSN, microvillar, and sustentacular), excluding Bowman's glands. Data were normalized with sc.pp.normalize() with a target_sum of 1e4. Next, sc.tl.pca() was run, followed by sc.pp.neighbors() with 5 neighbors and 30 principal components. A plot was generated with sc.tl.draw_graph() followed by sc.pl.draw_graph(), with default settings. We performed denoising by running sc.tl.diffmap() followed by sc.pp.neighbors() with 5 neighbors. Data were reclustered with sc.tl.leiden with a resolution of 2.0. Then partition-based graph abstraction was run with sc.tl.paga() followed by sc.pl.paga(), then sc.tol.draw_graph(), and finally sc.pl.draw_graph(), all with default settings. Cell identities were analyzed with feature plots. Small clusters of cells that did not align with any of the known cell markers were filtered out. The process was rerun iteratively beginning with sc.tl.pca() for a total of three times to ensure purity of cell identities within the trajectory plot. To produce the trajectory marker heat map, data were logarithmized and then scaled with sc.pp.log1p() and sc.pp.scale() to allow for visualization of variably expressed genes on one

plot. Data were plotted with sc.pl.paga_path(), using default settings. All uniform manifold approximation and projection (UMAP) plots and featureplots were produced with normalized count matrices and plotted using sc.pl.umap().

Downstream Analysis of RNA-seq Samples

Concatenated bulk RNA-seq count matrices (19 ONB specimens, three normal OE), were loaded into R (v4.1.1) for further differential expression analysis. To compare gene expression between tumor grades, DESeq2 (v1.32.0) was run, using default settings. Counts were normalized with counts(dds, normalized = T). Box plots of counts were produced with plotCounts(), and stat_compare_means() was run to perform Kruskal–Wallis testing among all three groups, followed by *post hoc* Dunn test for multiple comparisons.

Survival (v3.3-1) and survminer (v0.4.9) were used to perform survival curve analysis based on gene expression. We first created a matrix with survival data from each of the 19 patients with ONB using available data from Classe and colleagues, 2018 (19). A DESeq2 object using only the 19 ONB bulk RNA-seq count matrices was produced as described above, with normalized counts. For a given gene, we then calculated the median expression among all 19 tumors. We divided the dataset into a "low" and "high" expression group using approximately the median value as a cutoff. Then, a survival model integrating the combined count matrix with the survival outcomes matrix was created using survfit(), with overall survival as the outcome measure. A log-rank test *P*-value was calculated using surv_pvalue() and the Kaplan–Meier graph was plotted with ggsurvplot().

IHC

Human samples were obtained under approved protocol from Institutional Review Board at Duke University (Durham, NC), #Pro00088414. Normal olfactory mucosal and ONB biopsies were collected in the operating room on ice in Hanks' Balanced Salt Solution (Gibco) +10% FBS. Surgical specimens were washed twice in PBS and fixed for approximately 3 hours in 4% paraformaldehyde (Sigma). Tissue was washed two times in PBS and incubated at 4°C for 3–5 days in 30% sucrose, 250 mmol/L Ethylenediaminetetraacetic acid (EDTA), and PBS. Specimens were flash frozen with liquid nitrogen in optimal cutting temperature (VWR), cut into 10-μm-thick sections using a CryoStar NX50 cryostat (Thermo Fisher Scientific), and collected on Superfrost plus glass slides (Thermo Fisher Scientific).

Tissue sections on slides were incubated in PBS for 5 minutes, followed by dehydration-rehydration in ethanol (1 minute 70% ethanol, 1 minute 95% ethanol, 1 minute 100% ethanol, 1 minute 95% ethanol, 1 minute 70% ethanol, 5 minutes PBS). Antigen retrieval was performed using citrate-based unmasking solution (Vector Laboratories) by steaming for 45 minutes. Tissue was washed once in PBS for 5 minutes. Sections were blocked with blocking buffer (5% normal goat serum, 0.1% TritonX-100 in PBS) for 1 hour in a moist chamber at room temperature. Tissue was incubated in primary antibody overnight at 4°C in a moist chamber diluted in blocking buffer with the following dilutions: Anti-Tubulin β3 (BioLegend, clone TUJ1, 1:500, RRID: AB_2313773); Anti-OMP (Santa Cruz Biotechnology, sc-365818, 1:500, RRID: AB_10842164); Anti-EZH2 (Abcam, clone 11/EZH2, 1:500, RRID: AB_10694683); Anti-EED (Cell Signaling Technologies, clone E4L6E, 1:50, RRID: AB_2923355); Anti-SOX2 (eBioscience, 14-9811, 1:50, RRID: AB_11219471); Anti-SOX9 (Cell Signaling Technologies, clone D8G8H, 1:50, RRID: AB_2665492); Anti-S100B (Abcam, clone 4C4.9, 1:100, RRID: AB_304258); Anti-Ki-67 (DAKO, mouse, clone MIB-1, 1:50, RRID: AB_2631211); Anti-Ki-67 (Abcam, ab15580, rabbit, 1:250, RRID: AB_443209). Sections were washed three times for 5 minutes each in PBS+0.3% TritonX-100 and incubated with appropriate fluorescent conjugated secondary antibody (Jackson ImmunoResearch) for 45 minutes at room temperature. For EZH2 and SOX9 antibodies, in place of fluorescent conjugated secondary antibody incubation, a TSA fluorescein system (Akoya Biosciences) was used to amplify signal. Tissue was washed three times for 5 minutes each in PBS+0.3% TritonX-100, incubated for 3 minutes in Hoechst nuclear stain (1:1,000 in H_2O, Thermo Fisher Scientific), and mounted with Vectashield (Vector Laboratories). Images were acquired using a Leica DMi8 microscope system, and Leica Application Suite X software (v3.7.5). Images were processed in ImageJ (v2.3.0) and scale bars were drawn using metadata in the .lif image files.

Statistical Analysis

All statistical tests were performed in R (v4.1.1) or Graphpad Prism 9. Datasets were assessed for normal distribution, and the appropriate follow-up test (ANOVA vs. nonparametric) was performed. Given that this study was a retrospective analysis utilizing all publicly available bulk RNA-seq data on ONB, power analysis, randomization, and blinding were not appropriate or necessary.

Data Availability

All datasets used in this article are publicly available on GEO, with accession numbers listed above. Code used in analysis and to produce figures has been deposited on Github at https://github.com/Goldstein-Lab.

Results

Pseudodeconvolution of Normal OE and ONB Bulk RNA-seq Samples

Given that ONBs are rare tumors, it is not surprising that single-cell transcriptomic datasets that encompass the diversity of low- to high-grade tumors are not yet available. Therefore, we sought to take advantage of recent innovations in transcriptomic biocomputational analyses by deconvoluting cell type signatures (26) in available bulk RNA-seq ONB datasets (19), using a robust single-cell reference atlas from normal human olfactory mucosa. Traditionally, bulk RNA-seq deconvolution involves training a model with a scRNA-seq dataset from the same tissue type. The model learns patterns of aggregate gene expression across different cell identities, and then analyzes bulk RNA-seq datasets for similar expression patterns (ref. 26; Fig. 1). The output is a relative proportion of each cell identity (as annotated in the scRNA-seq reference dataset) within a given bulk RNA-seq sample. Here we refer to our analysis as pseudodeconvolution, because the scRNA-seq training dataset is from normal olfactory mucosa cells, not ONB. This is highly useful, because the deconvolution can identify patterns of gene expression within ONBs that map directly to specific cell states within the tissue from which tumors arise. As a control, we deconvoluted three bulk RNA-seq samples obtained from normal human OE.

Across the three normal OE samples, we observed similar patterns of cell type abundance, with approximately 10% neural lineage cells, 10% immune cells, 20% Bowman's glands, and a significant proportion mapping to respiratory cell types, which is expected given that the OE is generally interspersed with patches of respiratory epithelium in humans (Fig. 2A). When we explored deconvolution of low- and high-grade ONB samples, we identified a clear enrichment of OE cell types in ONB (Fig. 2A). Specifically, there is a significantly greater proportion of GBCs in high-grade ONB compared with normal OE, and significantly fewer mature OSNs, as compared with low-grade tumors (Fig. 2B).

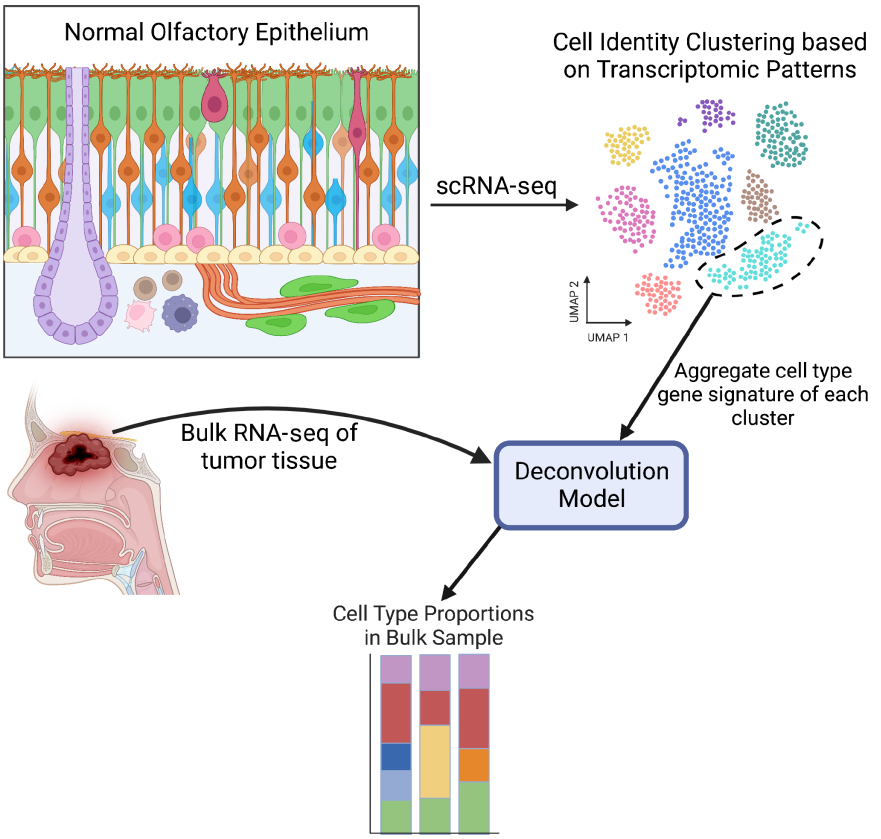

FIGURE 1 Schematic of the deconvolution workflow. Diagram of normal OE in the top left colored by cell identity (HBC: yellow; GBC: pink; immature OSN: blue; mature OSN: orange; Sustentacular: green; Bowman's Gland: purple; Olfactory ensheating cell:lime green in lamina propria; immune cells: round cells in lamina propria). The schematic depicts the two main inputs into the deconvolution model: a reference scRNA-seq dataset along with bulk RNA-seq data. The output is a stacked bar graph with estimated proportions of cell identity per bulk RNA-seq sample.

Note, GBCs generally represent approximately 0.25% of cells captured in our normal adult olfactory mucosa biopsies, so they artificially appear absent from deconvolution of bulk RNA-seq samples given the contribution of their unique transcripts to overall reads. Sustentacular and microvillar cells, which can both arise from GBCs, were either decreased (sustentacular) or remained the same (microvillar) in ONBs, when compared with normal OE. Interestingly, Bowman's glands, which were found to be relatively abundant (20% proportion) in normal olfactory mucosa biopsies, trended down with higher tumor grade, with significantly fewer Bowman's gland gene signatures in high-grade ONBs (Fig. 2B). Similarly, compared with low-grade tumors, high-grade ONBs had significantly fewer olfactory ensheathing cells, a neural crest–derived glial cell similar to nonmyelinating Schwann cells. We did not observe a significant difference in proportions of proliferative respiratory suprabasal cells, confirming that the model uses more than a simple panel of proliferation genes to map tumor cell identity. Finally, there have been conflicting data on the existence of a positive correlation between tumor grade and degree of T-cell infiltration in ONB (19, 27, 28). With our model, we find that higher grade ONBs do have a higher proportion of CD8 T cells.

These data suggest that while lower grade ONBs do contain more differentiated neural components, they may also have significant proportions of other differentiated cell-type lineages including Bowman's glands and olfactory ensheathing cells. It is also interesting to note that higher grade tumors do not map entirely to rapidly proliferating basal cells, and that they still contain significant proportions of neuronal cell type signatures. While the available bulk RNA-seq datasets are felt to contain predominantly tumor cells, it is impossible to exclude some contribution of normal overlying surface epithelium, either olfactory or respiratory, which could contribute to overall transcripts.

An important consideration is that IDH2 mutations in ONB are uncommon and that Classe and colleagues, 2018 report an association between IDH2 mutations and positive cytokeratin staining by IHC (19). Therefore, it is possible that IDH2 mutant tumors could be sinonasal undifferentiated carcinomas (SNUC), which are highly positive for cytokeratins and more commonly harbor IDH2 mutations (29). To explore the possibility that these tumors may be confounding the results of our model, we reanalyzed our model outputs with the two IDH2 ONB mutant tumors (both high grade) separated out into their own category (Supplementary Fig. S1). Overall, with these tumors excluded, we did not observe any significant changes in cell type proportion estimates. Furthermore, we analyzed RNA expression of common histology markers of SNUC (cytokeratins; Supplementary Fig. S2A), small cell neuroendocrine carcinoma (Supplementary Fig. S2B), and ONB (Supplementary Fig. S2C). We did not observe a significant increase in expression of any keratin genes in IDH2 mutant versus high-grade wild-type tumors. ONB marker genes tend to decrease in expression in high-grade versus low-grade tumors, but there was no significant difference between high-grade IDH2 wild-type and IDH2 mutant tumors. Together, these RNA expression data do not suggest that the IDH2 mutant tumors in this dataset are SNUCs misclassified as ONB.

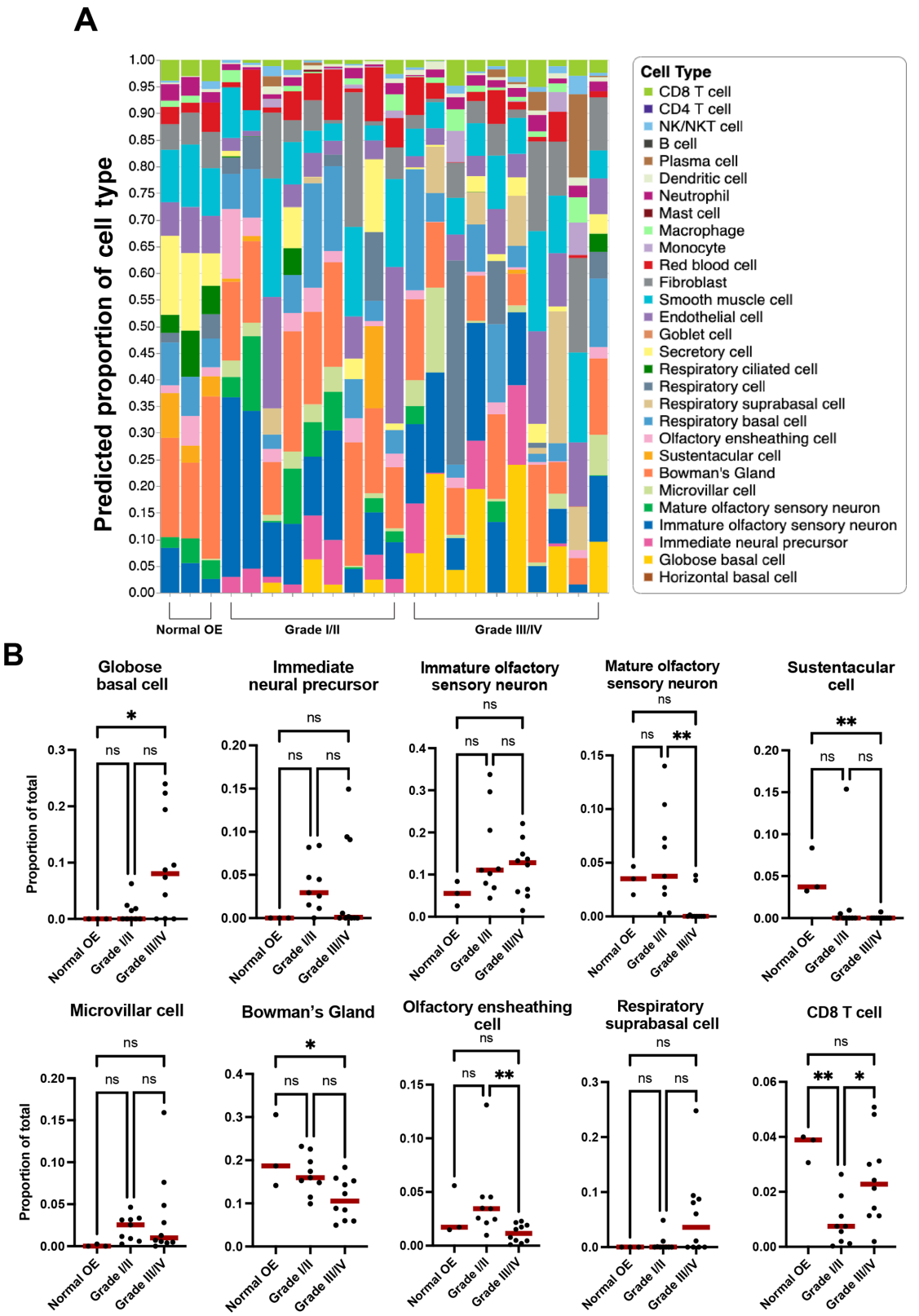

FIGURE 2 Pseudodeconvolution of ONB bulk RNA-seq defines proportions of cell type–specific transcriptomics across low- and high-grade tumors. **A,** Stacked bar chart depicts predicted proportions of cell types in bulk tumors when mapped to control adult human olfactory mucosa using the deconvolution model. **B,** Statistical differences in selected ONB cellular composition, based on one-way ANOVA followed by *post hoc* Tukey test (*, $P < 0.05$; **, $P < 0.01$).

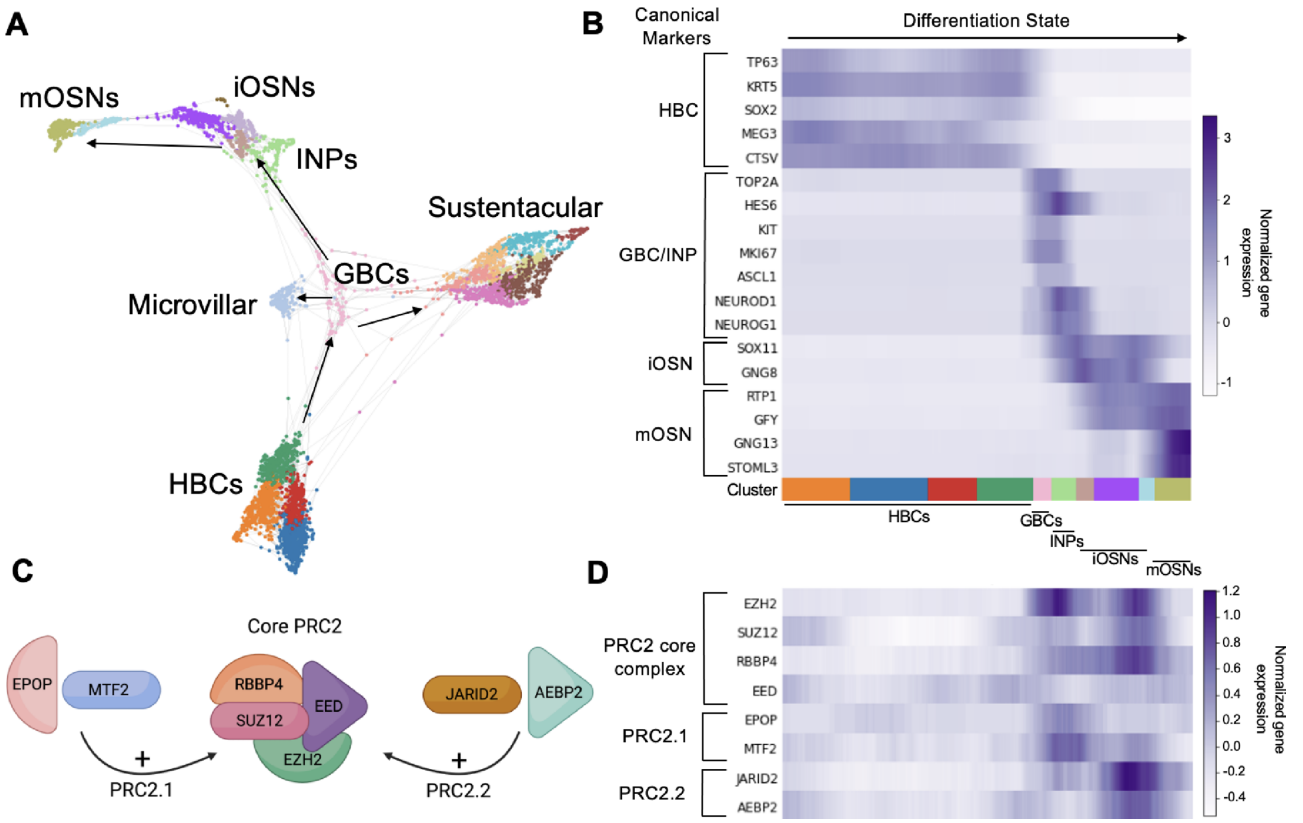

FIGURE 3 Patterns of gene expression in the normal differentiating OE. **A,** Trajectory UMAP depicting differentiation states across pseudotime, in seven normal olfactory mucosa biopsies scRNA-seq from Durante and colleagues, 2020 and Oliva and colleagues, 2021 (13, 24). **B,** Heat map showing canonical cell type–specific markers for selected OE cell stages. **C,** Schematic showing that the core PRC2 protein complex can combine with either EPOP+MTF2 to form PRC2.1 or with JARID2+AEBP2 to form PRC2.2. **D,** Heat map showing PRC2 gene expression (and IDH2). (HBC: horizontal basal cell; GBC: globose basal cell; INP: immediate neuronal precursor; iOSN: immature olfactory sensory neuron; mOSN: mature olfactory sensory neuron; PRC2: Polycomb repressive complex 2).

Trajectory Analysis in Normal OE Samples Reveals Potential Regulators of Tumorigenesis

Given the olfactory cell lineages identified in both low- and high-grade ONBs, we hypothesized that regulatory mechanisms controlling normal olfactory proliferation and/or differentiation are likely to play a role in ONB tumorigenesis. One likely candidate is the polycomb family. PRC2 is an epigenetic modifier that regulates transcription in developing and adult stem cell niches via modulation of chromatin structure. We have previously identified expression of core PRC2 proteins, including EZH2, EED, and SUZ12, in OE sensory lineages, and EZH2 histone methyltransferase activity appears to regulate murine GBC proliferation (30, 31). Therefore, we utilized trajectory analysis on our single-cell dataset containing seven normal human olfactory mucosal biopsies to visualize where PRC2 gene expression is upregulated along human OE cell differentiation trajectories (Fig. 3A). We identified cellular states across three different lineage trajectories and used previously identified cell type–specific markers to confirm cell identity (ref. 13; Fig. 3B). Specifically, we identified a cluster of HBCs ($TP63^+$, $KRT5^+$) as the starting point of the differentiation trajectory. From here, trajectories could either progress along pseudotime toward a fully mature neuron (mOSN, $RTP1^+$, $GNG13^+$), a microvillar cell ($ASCL3^+$), or a sustentacular cell cluster ($SOX2^+$, $ERMN^+$). Intervening GBC and INP stages were also identified.

Having established an *in silico* model of human OE differentiation, we next focused on transcripts for core PRC2 components (EZH2, SUZ12, EED, RBBP4) or subunits specific to PRC2.1 (MTF/PCLs, EPOP) or PRC2.2 (JARID2, AEBP2) complexes (Fig. 3C; ref. 32). Distinct PRC2 complexes with unique subunit composition confer different transcriptional regulation to certain cell phenotypes in other self-renewing systems, such as the skin or hematopoietic system (33); however, these potential roles in the adult OE remain to be defined. As a cell differentiates from an HBC into a mature OSN, we observed a pattern of significantly increased expression in PRC2 transcripts in GBC identities (Fig. 3D). Of note, this first peak is associated with a single peak in EPOP and MTF2, two constituents of PRC2.1. As cells continue on to INPs, there is a minor decrease in many of these genes, followed by a second peak in expression prior to an iOSN maturing into an mOSN; this second peak, in contrast to the first, corresponds with a single peak in JARID2 and AEBP2, constituents of PRC2.2. Once a cell is a fully mature neuron, there is consistently low expression of PRC2 transcripts. Unlike in the neuronal trajectory, we did *not* detect differences in expression of Polycomb subunits along the sustentacular differentiation trajectory, consistent with a neuron lineage–specific function for PRC2.

We also queried expression of IDH2 along these trajectories, given that mutations in IDH2 have been one of the only recurrent mutations reported in high-grade ONB (19). We find that like PRC2 genes, IDH2 expression peaks at

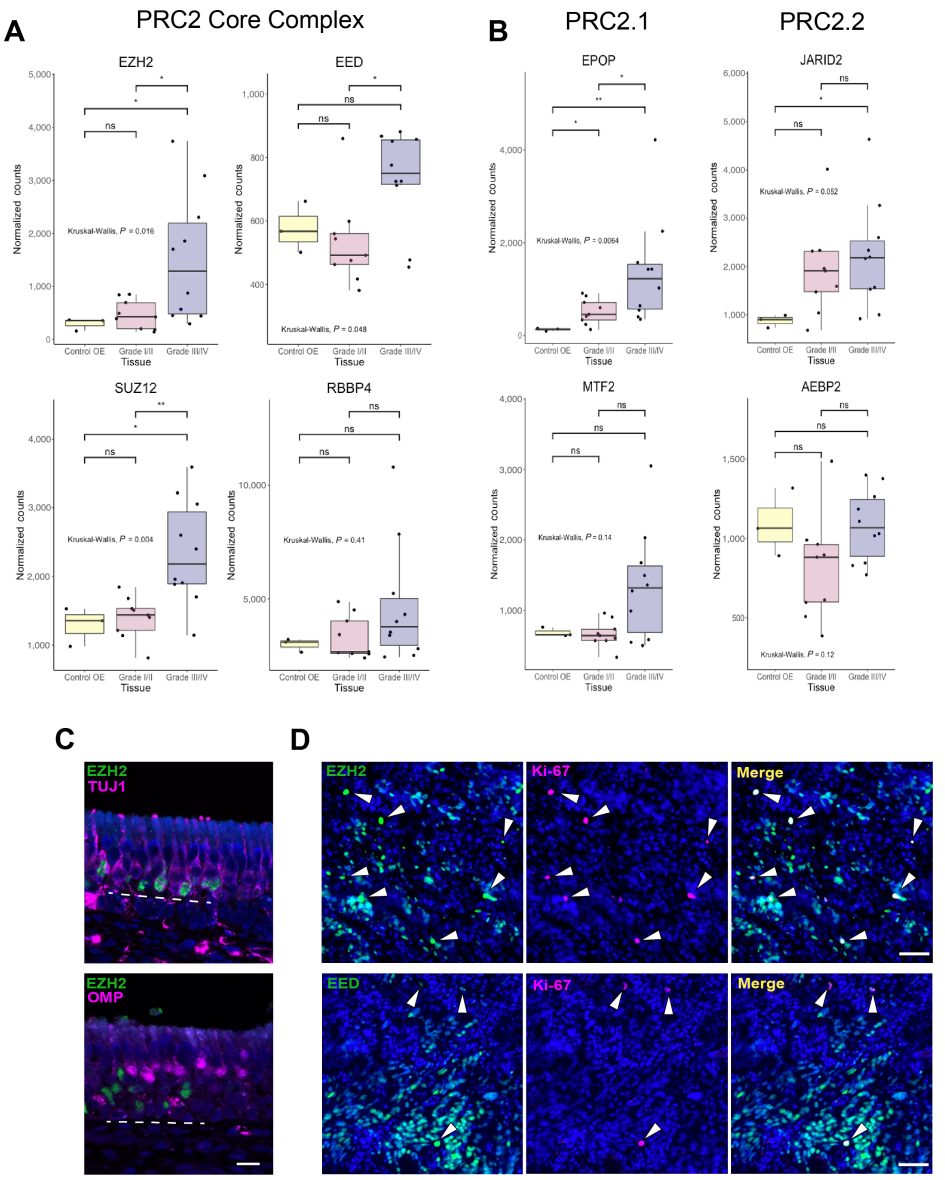

FIGURE 4 PRC2 complex expression in ONB. **A,** PRC2 transcripts in the core complex are mostly upregulated in high-grade ONB. **B,** EPOP expression is significantly increased in high-grade ONB compared with low grade, with no differences between low and high grade in proteins that form the PRC2.2 complex. For A and B, statistical significance assessed by Kruskal–Wallis test with *post hoc* Dunn test for multiple comparisons (*, $P < 0.05$; **, $P < 0.01$). **C,** EZH2 is present in basal cells and immature neurons (TUJ1$^+$) but not in mature neurons (OMP$^+$) in the normal human OE. **D,** Immunohistochemically, Ki-67$^+$ cells are nearly uniformly positive for EZH2 and EED in a grade I ONB. Scale bars in C and D are 50 μm.

the GBC to INP cell identity (Fig. 3D). This finding serves as further confirmation that higher grade ONBs are likely expressing cellular programs that most closely resemble those of GBCs. Furthermore, our trajectory analysis provides additional detail regarding selective PRC2 gene expression in the GBC/iOSN cellular states in human OE.

PRC2 is Associated with Proliferation in ONB

Because PRC2 is active in proliferative neural progenitors in the mouse (30, 31) and normal human OE, we asked whether there was any link between PRC2 expression and proliferation in ONB. Using the previously published datasets of bulk RNA-seq from ONBs and normal olfactory mucosa, we divided samples into normal OE, Hyams grade I/II ONB, and Hyams grade III/IV ONB, as in Fig. 2B. Higher grade tumors have a greater percentage of Ki-67$^+$ cells, reflective of increased proliferative activity. We compared expression of PRC2 transcripts (EZH2, EED, SUZ12, RBBP4) across these three groups and found a significant increase in expression of EZH2, EED, and SUZ12 in the higher grade tumors compared with lower grade (Fig. 4A). Because we observed that accessory proteins associated with PRC2.1 (EPOP, MTF2) peaked at the GBC/INP state and those associated with PRC2.2 (JARID2, AEBP2) peaked at the iOSN state, we asked whether there were detectable differences across ONB grade. Interestingly, there is a significant increase in EPOP expression in high-grade compared with low-grade tumors, with no differences between tumor grade in

PRC2.2 protein expression (Fig. 4B). This suggests that PRC2.1 specifically may play a role in ONB malignancy. Similar findings were observed when IDH2 mutant tumors were separated from analysis (Supplementary Fig. S3).

Next, we used IHC to stain for PRC2 proteins. We first confirmed presence of EZH2 protein in the normal human OE, and validated that its expression is limited to basal cells and immature neurons (TUJ1$^+$; Fig. 4C). We then examined PRC2 protein expression in an ONB sample and costained with anti-Ki-67 to assess proliferation. Although our staining was performed on a grade I tumor, Ki-67$^+$ cells were identified throughout the sample (Fig. 4D). Staining revealed that nearly all Ki-67$^+$ cells were also EZH2$^+$. Similarly, most Ki-67$^+$ cells stained positive for EED. These results suggest that expression of core PRC2 proteins is associated with proliferation in ONB both at the RNA and protein level.

ONB Expression of Canonical Bowman's Gland or Olfactory Ensheathing Glia Transcripts Correlates with Favorable Prognosis

With the finding that higher grade tumors have significantly decreased expression of Bowman's gland and olfactory ensheathing cell transcriptional identities, we asked whether expression of key marker genes of these cell types was associated with favorable prognosis. Differential expression analysis in our single-cell atlas of seven normal human olfactory mucosa samples identifies PLP1 and S100B as genes unique to olfactory ensheathing cells, while high levels of SOX9 is specific to Bowman's glands. SOX9 expression is, however, also present in the subset of Trpm5$^+$ microvillar cells (Fig. 5A). To assess impact on prognosis, we queried the ONB bulk RNA-seq dataset and divided tumors into low or high expression groups based on whether expression of a given gene fell below or above the median expression of the gene across all tumors. Then, we generated Kaplan–Meier plots and ran log-rank tests to determine statistical significance. Of particular interest, we found that tumors with higher expression of PLP1, S100B, and SOX9 all confer a statistically significant increase in survival (Fig. 5B). Because TRPM5$^+$ microvillar cells also express SOX9, we ran a similar analysis with TRPM5 expression but did not observe any differences in survival, suggesting that the finding are related to SOX9$^+$ Bowman's gland cells, or a de-differentiated microvillar cell state that does not express TRPM5 (Fig. 5B).

As controls, we assessed the effects of Hyams grade, Dulguerov T stage, and MKI67 expression (gene for Ki67 protein) on survival in these datasets. Hyams grade and Dulguerov T stage were both approaching but did not achieve statistical significance, while higher MKI67 expression was associated with significantly worse survival (Supplementary Fig. S4). We also analyzed the "high" and "low" gene expression populations from each survival plot in Fig. 5B within the context of tumor grade, stage, and Ki-67 expression to assess for possible confounders (Supplementary Table S1). There were no strong associations between cohorts with a favorable prognosis and grade/stage of the tumor, with the exception of MKI67. In contrast, the PLP1 low, S100B low, and SOX9 low groups all had higher average MKI67 expression, suggesting that expression of these genes tends to inversely correlate with Ki-67 mRNA expression (Supplementary Table S1). It is important to note, however, that we did not observe 100% concordance between these populations with favorable prognosis and the MKI67 low population. It is possible that MKI67 expression may, to an extent, be confounding survival outcomes based on PLP1, S100B, and SOX9 gene expression. Regardless, our analysis suggests that, in this ONB dataset, PLP1, S100B, and SOX9 expression levels are, at a minimum, strong markers for survival as compared with the standard grading and staging systems.

For further validation of these prognostic markers, we analyzed S100B and SOX9 protein in an ONB tumor by IHC. Our staining confirms the expression of nuclear SOX9 or SOX2 protein in ONB, and these transcription factors are mutually exclusive (Fig. 5C). Also, we did not identify coexpression of Ki-67 in SOX9$^+$ cells. We also confirmed the expression of S100B protein in ONB and do identify occasional coexpression of Ki-67 in S100B$^+$ cells (Fig. 5D). Of interest, in normal adult human olfactory mucosa, S100B expression is highly specific to olfactory ensheathing glia, as it is in rodent (34, 35). Although prior reports have referred to S100B in ONB as a marker for sustentacular cells (36), we are not aware of any evidence in mouse or human that this protein is present in sustentacular cells (Fig. 5A). We conclude that S100B expression in ONB is likely reflective of the presence of ensheathing glia, or possibly other neural crest–derived elements related embryonically to the surrounding mesenchyme.

Discussion

The findings presented here have several implications regarding mechanisms of ONB tumor growth and prognosis. By leveraging new insights from the adult human olfactory epithelial stem cell niche and new biocomputational techniques, we sought to better understand the biology of a rare and clinically challenging olfactory cleft neoplasm. There are limitations to our study that must be acknowledged, largely related to the fact that ONB is a rare tumor. Our deconvolution method utilizes normal olfactory epithelial tissue, not tumors, to predict cell-type proportions. This makes it difficult to determine the precise amount of tumor tissue versus nearby healthy tissue within each bulk RNA-seq sample. Because no representative single-cell datasets of ONB exist, it is not currently possible to utilize a deconvolution model to answer this question. Thus, it is important to consider that there could be variability in amount of tumor and normal OE from sample to sample. We believe that our approach which averages proportions across nine low-grade and 10 high-grade tumors helps to mitigate this potential variability. An additional limitation is that we were only able to perform immunofluorescence staining on one ONB due to access to limited tissue specimens. These initial validations should be followed-up in future studies of larger ONB datasets, including generation of robust single-cell datasets containing high- and low-grade ONB.

Several challenges exist when considering ONB treatment. At present, no accepted or standard targeted/biologic therapy for ONB has been identified. Therefore, higher grade tumors have been managed with conventional regimens often using cisplatin and etoposide, or cyclophosphamide/vincristine, along with surgery and radiation (2, 37). Significant potential morbidity must be considered with achieving widely negative margins of surgical resection, due to anatomy of the olfactory cleft and adjacent structures. Morbidity can involve need for resection of orbit or intracranial contents. Furthermore, bilateral anterior skull base resection and removal of olfactory bulbs renders patients permanently and irreversibly anosmic. Thus, the identification of targets for biologic or novel therapies, with potential to be effective in advanced ONB, is needed.

The findings presented here provide a rationale for potential treatment strategies. Leveraging advances in our understanding of the mechanisms regulating olfactory neurogenesis and, specifically, GBC proliferation and differentiation, and mapping ONB transcriptional profiles to normal adult human olfactory datasets at single-cell resolution, we identify new insights regarding ONB. A key finding involves a likely role for PRC2 in proliferative ONB cells. It is intriguing to consider that the enzymatically active PRC2 subunit, EZH1/2, is a druggable target (38). Indeed, PRC2 is a treatment focus for several malignancies,

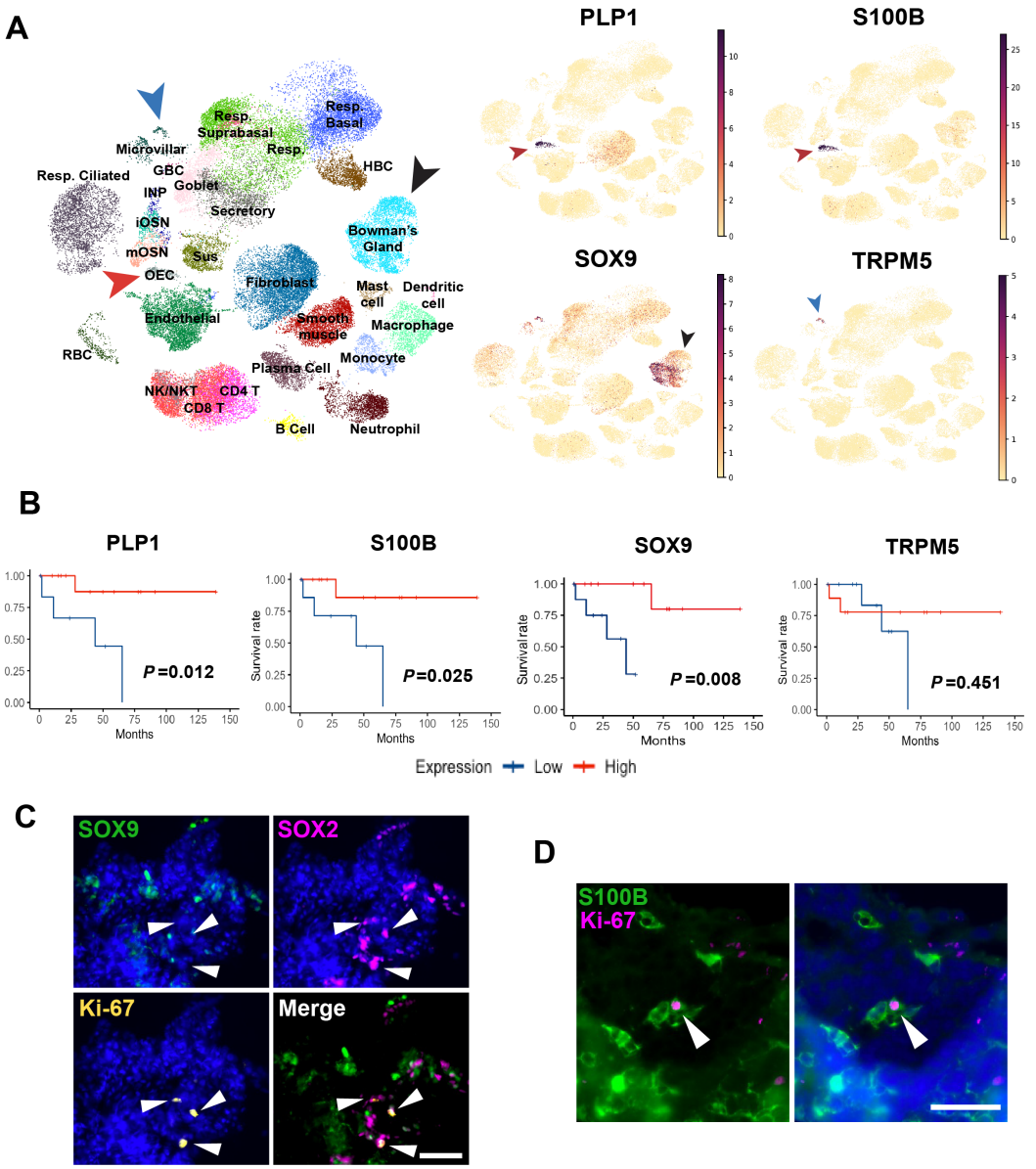

FIGURE 5 Glandular and olfactory ensheathing cell markers are present in low-grade ONB and are associated with increased survival. **A,** UMAP visualization of non-tumor olfactory mucosa scRNA-seq data depicts the cell type–specific expression of selected transcripts. PLP1 and S100B are expressed in olfactory ensheathing cells (OEC, red arrow); SOX9 is highly expressed in Bowman's glands (black arrow) and the TRPM5$^+$ subset of microvillar cells (blue arrow). Scale bar shows normalized counts. **B,** Kaplan–Meier survival curves showing significant survival advantage in ONB tumors with higher expression of Bowman's gland and OEC markers. Statistical significance determined by log-rank test. **C,** SOX9$^+$ cells are rarely Ki-67$^+$ and do not colocalize with SOX2. In contrast, some SOX2$^+$ cells show evidence of proliferation based on Ki-67 staining (arrowheads). **D,** The presence of S100B$^+$ cells in a grade I ONB. Ki-67 costaining confirms the presence of the occasional proliferative S100B$^+$ cell (arrowhead). In A, resp = respiratory; RBC = red blood cell; sus = sustentacular; in C and D, scale bar = 50 μm.

including hematologic and solid tumors (39, 40). In considering drug development, there is also a focus on potential PRC2-independent roles for EZH2 in cancer (41).

In addition to potential utility in cases of ONB metastasis or recurrence, a targeted ONB therapy may be useful as a neoadjuvant drug for bulky ONB tumors, to permit removal via a hemi-skull base resection that could spare the contralateral olfactory structures and thus preserve olfaction. Our results provide a basis for further research regarding targeted therapy for ONB.

Another novel finding from our analysis is the potential utility of specific prognostic markers in ONB. Specifically, we found here that expression of the Bowman's gland and TRPM5+ microvillar cell transcription factor SOX9, and also the olfactory ensheathing glia markers S100B or PLP1, all correlate significantly with improved prognosis in this dataset including 19 ONB subjects. Considering the low incidence of ONB, our approach mapping existing transcriptional datasets to robust normal human olfactory single-cell data provided a means to identify cell type–specific transcripts of interest for survival data query.

Together, our findings suggest important mechanisms contributing to ONB tumor growth, as well as pathologic markers for prognosis. We anticipate that these insights will be useful in guiding further translational studies. More broadly, these mechanistic insights will be helpful in considering development of future personalized approaches to the management of this rare and challenging tumor.

Authors' Disclosures

N. Osazuwa-Peters reports grants from NIH/NIDCR and other from Navigating Cancer outside the submitted work. B.J. Goldstein reports grants from NIH during the conduct of the study. No disclosures were reported by the other authors.

Authors' Contributions

J.B. Finlay: Conceptualization, data curation, software, formal analysis, investigation, visualization, methodology, writing-original draft, writing-review and editing. **R. Abi Hachem:** Resources, data curation, writing-review and editing. **D.W. Jang:** Resources, data curation, writing-review and editing. **N. Osazuwa-Peters:** Writing-review and editing. **B.J. Goldstein:** Conceptualization, resources, software, formal analysis, supervision, funding acquisition, validation, investigation, methodology, writing-original draft, project administration, writing-review and editing.

Acknowledgments

We thank all of the patients who played a role in making this study possible. Graphical schematics in this article were created with BioRender. This work was funded by NIH grants DC016859 and DC018371, to B.J. Goldstein.

Note

Supplementary data for this article are available at Cancer Research Communications Online (https://aacrjournals.org/cancerrescommun/).

Received January 05, 2023; revised March 13, 2023; accepted May 11, 2023; published first June 06, 2023.

References

1. Berger L, Luc R, Richard D. L'esthesioneuroepitheliome olfactif. Bulletin de l'Association Française pour l'étude du Cancer 1924;13: 410-21.
2. Ow TJ, Bell D, Kupferman ME, Demonte F, Hanna EY. Esthesioneuroblastoma. Neurosurg Clin N Am 2013;24: 51-65.
3. Hyams VJ, Batsakis JG, Michaels L; Armed Forces Institute of Pathology. Tumors of the upper respiratory tract and ear. Atlas of tumor pathology; 2nd ser, fasc 25. Washington (DC): Armed Forces Institute of Pathology; 1988.
4. Tajudeen BA, Arshi A, Suh JD, St John M, Wang MB. Importance of tumor grade in esthesioneuroblastoma survival: a population-based analysis. JAMA Otolaryngol Head Neck Surg 2014;140: 1124-9.
5. Kadish S, Goodman M, Wang CC. Olfactory neuroblastoma. A clinical analysis of 17 cases. Cancer 1976;37: 1571-6.
6. Dulguerov P, Allal AS, Calcaterra TC. Esthesioneuroblastoma: a meta-analysis and review. Lancet Oncol 2001;2: 683-90.
7. Eden BV, Debo RF, Larner JM, et al. Esthesioneuroblastoma. Long-term outcome and patterns of failure–the University of Virginia experience. Cancer 1994;73: 2556-62.
8. Thawani R, Kim MS, Arastu A, Feng Z, West MT, Taflin NF, et al. The contemporary management of cancers of the sinonasal tract in adults. CA Cancer J Clin 2023;73: 72-112.
9. McElroy EA Jr, Buckner JC, Lewis JE. Chemotherapy for advanced esthesioneuroblastoma: the Mayo Clinic experience. Neurosurgery 1998;42: 1023-7.
10. Bell D, Saade R, Roberts D, Ow TJ, Kupferman M, DeMonte F, et al. Prognostic utility of Hyams histological grading and Kadish-Morita staging systems for esthesioneuroblastoma outcomes. Head Neck Pathol 2015;9: 51-9.
11. Loy AH, Reibel JF, Read PW, Thomas CY, Newman SA, Jane JA, et al. Esthesioneuroblastoma: continued follow-up of a single institution's experience. Arch Otolaryngol Head Neck Surg 2006;132: 134-8.
12. Kaur RP, Izumchenko E, Blakaj DM, Mladkova N, Lechner M, Beaumont TL, et al. The genomics and epigenetics of olfactory neuroblastoma: a systematic review. Laryngoscope Investig Otolaryngol 2021;6: 721-8.
13. Durante MA, Kurtenbach S, Sargi ZB, Harbour JW, Choi R, Kurtenbach S, et al. Single-cell analysis of olfactory neurogenesis and differentiation in adult humans. Nat Neurosci 2020;23: 323-6.
14. Caggiano M, Kauer JS, Hunter DD. Globose basal cells are neuronal progenitors in the olfactory epithelium: a lineage analysis using a replication-incompetent retrovirus. Neuron 1994;13: 339-52.
15. Schwob JE, Huard JM, Luskin MB, Youngentob SL. Retroviral lineage studies of the rat olfactory epithelium. Chem Senses 1994;19: 671-82.
16. Huard JM, Youngentob SL, Goldstein BJ, Luskin MB, Schwob JE. Adult olfactory epithelium contains multipotent progenitors that give rise to neurons and non-neural cells. J Comp Neurol 1998;400: 469-86.
17. Fletcher RB, Das D, Gadye L, Street KN, Baudhuin A, Wagner A, et al. Deconstructing olfactory stem cell trajectories at single-cell resolution. Cell Stem Cell 2017;20: 817-30.
18. Forni PE, Taylor-Burds C, Melvin VS, Williams T, Wray S. Neural crest and ectodermal cells intermix in the nasal placode to give rise to GnRH-1 neurons, sensory neurons, and olfactory ensheathing cells. J Neurosci 2011;31: 6915-27.
19. Classe M, Yao H, Mouawad R, Creighton CJ, Burgess A, Allanic F, et al. Integrated multi-omic analysis of esthesioneuroblastomas identifies two subgroups linked to cell ontogeny. Cell Rep 2018;25: 811-21.
20. Holbrook EH, Wu E, Curry WT, Lin DT, Schwob JE. Immunohistochemical characterization of human olfactory tissue. Laryngoscope 2011;121: 1687-701.
21. Trojanowski JQ, Lee V, Pillsbury N, Lee S. Neuronal origin of human esthesioneuroblastoma demonstrated with anti-neurofilament monoclonal antibodies. N Engl J Med 1982;307: 159-61.
22. Carney ME, O'Reilly RC, Sholevar B, Buiakova OI, Lowry LD, Keane WM, et al. Expression of the human Achaete-scute 1 gene in olfactory neuroblastoma (esthesioneuroblastoma). J Neurooncol 1995;26: 35-43.
23. Olender T, Keydar I, Pinto JM, Tatarskyy P, Alkelai A, Chien M-S, et al. The human olfactory transcriptome. BMC Genomics 2016;17: 619.
24. Oliva AD, Gupta R, Issa K, Abi Hachem R, Jang DW, Wellford SA, et al. Aging-related olfactory loss is associated with olfactory stem cell transcriptional alterations in humans. J Clin Invest 2022;132: e155506.
25. Finlay JB, Brann DH, Abi-Hachem R, Jang DW, Oliva AD, Ko T, et al. Persistent post-COVID-19 smell loss is associated with inflammatory infiltration and altered olfactory epithelial gene expression. bioRxiv 2022; 2022.04.17.488474.
26. Erdmann-Pham DD, Fischer J, Hong J, Song YS. Likelihood-based deconvolution of bulk gene expression data using single-cell references. Genome Res 2021;31: 1794-806.
27. Zhu T, Liu J, Beck S, Pan S, Capper D, Lechner M, et al. A pan-tissue DNA methylation atlas enables in silico decomposition of human tissue methylomes at cell-type resolution. Nat Methods 2022;19: 296-306.

28. London NR Jr, Rooper LM, Bishop JA, Xu H, Bernhardt LJ, Ishii M, et al. Expression of programmed cell death ligand 1 and associated lymphocyte infiltration in olfactory neuroblastoma. World Neurosurg 2020;135: e187-93.
29. Riobello C, López-Hernández A, Cabal VN, García-Marín R, Suárez-Fernández L, Sánchez-Fernández P, et al. IDH2 mutation analysis in undifferentiated and poorly differentiated sinonasal carcinomas for diagnosis and clinical management. Am J Surg Pathol 2020;44: 396-405.
30. Goldstein BJ, Goss GM, Choi R, Saur D, Seidler B, Hare JM, et al. Contribution of Polycomb group proteins to olfactory basal stem cell self-renewal in a novel c-KIT+ culture model and *in vivo*. Development 2016;143: 4394-404.
31. Goldstein BJ, Choi R, Goss GM. Multiple polycomb epigenetic regulatory proteins are active in normal and regenerating adult olfactory epithelium. Laryngoscope Investig Otolaryngol 2018;3: 337-44.
32. Conway E, Jerman E, Healy E, Ito S, Holoch D, Oliviero G, et al. A family of vertebrate-specific polycombs encoded by the LCOR/LCORL genes balance PRC2 subtype activities. Mol Cell 2018;70: 408-421.
33. van Mierlo G, Veenstra GJC, Vermeulen M, Marks H. The complexity of PRC2 subcomplexes. Trends Cell Biol 2019;29: 660-71.
34. Au E, Roskams AJ. Olfactory ensheathing cells of the lamina propria *in vivo* and *in vitro*. Glia 2003;41: 224-36.
35. Barnett SC, Alexander CL, Iwashita Y, Gilson JM, Crowther J, Clark L, et al. Identification of a human olfactory ensheathing cell that can effect transplant-mediated remyelination of demyelinated CNS axons. Brain 2000;123: 1581-8.
36. Faragalla H, Weinreb I. Olfactory neuroblastoma: a review and update. Adv Anat Pathol 2009;16: 322-31.
37. Abdelmeguid AS, Bell D, Roberts D, Ferrarotto R, Phan J, Su SY, et al. Long-term outcomes of olfactory neuroblastoma: MD anderson cancer center experience and review of the literature. Laryngoscope 2022;132: 290-7.
38. Hanaki S, Shimada M. Targeting EZH2 as cancer therapy. J Biochem 2021;170: 1-4.
39. Yap TA, Winter JN, Giulino-Roth L, Longley J, Lopez J, Michot J-M, et al. Phase I study of the novel enhancer of zeste homolog 2 (EZH2) inhibitor GSK2816126 in patients with advanced hematologic and solid tumors. Clin Cancer Res 2019;25: 7331-9.
40. Chan HL, Morey L. Emerging roles for polycomb-group proteins in stem cells and cancer. Trends Biochem Sci 2019;44: 688-700.
41. Wang J, Yu X, Gong W, Liu X, Park K-S, Ma A, et al. EZH2 noncanonically binds cMyc and p300 through a cryptic transactivation domain to mediate gene activation and promote oncogenesis. Nat Cell Biol 2022;24: 384-99.